**Supplementary Information: CHIMIA, 2002, 76, 7/8, 661-668**

# Hybrid Microfluidic Device for High Throughput Isolation of Cells Using Aptamer Functionalized Diatom Frustules

Rashin Mohammadi,[†,‡] Mohammad Asghari,[†] Monika Colombo,[†] Zahra Vaezi,[‖] Daniel A. Richards,[†] Stavros Stavrakis,[†] Hossein Naderi-Manesh,[*‡] Andrew deMello[*†]

[†] Department of Chemistry and Applied Biosciences, ETH Zurich, Vladimir Prelog Weg 1, Zurich, 8093, Switzerland. [‡] Department of Nanobiotechnology, Faculty of Biological Sciences, Tarbiat Modarres University, Tehran, 14115-154, Iran. [‖] Department of Bioactive Compounds, Faculty of Interdisciplinary Science and Technologies, Tarbiat Modares University, Tehran, 14115-154, Iran

* e-mail: andrew.demello@chem.ethz.ch, naderman@modares.ac.ir

## Contents

# 1. Experimental Section

### Diatom culture

The *Chaetoceros sp.* diatom compound (obtained from the ABC microalgae bank, Iran, Bushehr) was cultured at 30°C with 200 $mE.m^{-2}.s^{-1}$ incident light in 250ml Erlenmeyer flasks containing Guillard's F/2 Medium (Merk, Zug, Switzerland). Diluted seawater with 25% salinity was used as the culture medium. The culture was placed for 16 hr under light and 8 hours under dark over 7 consecutive days.

### Diatom frustules preparation

The diatom biomass was concentrated by centrifugation of the culture for 5 minutes at 4000rpm. The mineral compounds were then removed from the medium. Afterwards $H_2O_2$ (30% in water, Sigma-Aldrich, Buchs, Switzerland) was added to the biomass and incubated for 4 hours at 90°C under reflux. Next, the samples were oxidized in 2M hydrochloric acid ( Sigma-Aldrich, Buchs, Switzerland) for 4 hours at 60°C. Frustules were then collected by centrifugation at 4000rpm for 5 minutes, washed five times with deionized water and stored at 4°C in deionized water.

### Magnetization of diatom frustules

Magnetic nanoparticles were synthesized using the co-precipitation method.[1] In brief, a 2:1 molar ratio of $FeCl_3$ and $FeCl_2$ (Sigma-Aldrich, Buchs, Switzerland) was introduced to a 50 ml deionized water solution under stirring at 80 °C. Next, 1M NaOH (Merk, Zug, Switzerland) was added dropwise (1ml/min) under nitrogen gas with vigorous stirring for 25 minutes. The magnetic nanoparticles were then rinsed with ethanol and deionized water and dried at 70 °C. Scanning electron microscopy (KYKY EM 3200, KYKY Co, Beijing, China) was used to determine the morphology and size of the magnetic nanoparticles. For the preparation of magnetic frustules, 5ml of iron oxide nanoparticles in deionized water (1g/L) were added to 0.1 gr/L diatom frustules in deionized water sonicated for 5 minutes and placed in a shaking incubator at room temperature for 24h. Finally the frustules coated with magnetic nanoparticles (mag@ DF) were collected using a Neodymium magnet and washed with deionized water 3 times.[2]

### Surface modification of magnetic diatom frustules with the TLS11a aptamer

An amino-modified DNA aptamer, TLS11a-$NH_2$, (5' $(CH)_6$ –AC AG CA TC CC CA TG TG AA CA AT CG CA TT GT GA TT GT TA CG GT TT CC GC CT CA TG GA CG TG CT G) was purchased from Microsynth (Zurich, Switzerland). mag@DF were functionalized with amino groups using an APTES solution. Specifically, 20mL of dried toluene (Sigma-Aldrich, Buchs Switzerland) were added to mag@DF (0.1gr/ml in PBS) and refluxed at 60 °C under vigorous stirring and nitrogen gas. Next, a 5% APTES (Sigma-Aldrich, Buchs Switzerland) solution in PBS (Phosphate Buffer Saline, Life technologies, Zug, Switzerland) was added to the mixture in a dropwise manner and stirred for 6 hours at 60°C. The mixture was then washed sequentially with toluene, isopropanol, and deionized water and stored in 10 ml of deionized water at 4°C.[3]

Aptamer functionalization was achieved using gluthardehyde as a linker for the Schiff base reaction. To this end, 1 ml of mag@DF-$NH_2$ (1 gr/l) was washed two times with PBS and

suspended into a 8% glutaraldehyde (Sigma-Aldrich, Buchs Switzerland) – PBS solution. The reaction took place at room temperature under continuous stirring for 4h. The reaction product (mag@DF-CHO) was washed two times with PBS to remove unbound glutaraldehyde. Afterwards, 100 μl from a 10 μM aptamer solution in PBS was first denatured at 95°C for 5 minutes and then renatured on ice for 15 minutes. For the conjugation of aptamers with mag@DF, 1ml of mag-frustules-CHO was added to 1ml of TLS11a-$NH_2$ solution (10μM in PBS) and constantly stirred at room temperature for 4h. Next, the product was washed two times with PBS, and a quenching solution (30mM glycine, 0.05% BSA in PBS) was added and stirred for 30 minutes. The final product was washed with PBS and kept in a storage buffer (0.5% BSA in PBS) at 4ºC.[4] The optical photoluminescent (PL) spectra of functionalized frustules were obtained using a Fluoromax spectrophotometer (Horiba, Neuhausen auf den Fildern, Germany). To characterize the functionalization of the final reactions products, Attenuated total reflectance Fourier transform infrared spectroscopy (ATR-FT-IR) spectra were obtained using a FTIR spectrophotometer (Bruker Alpha-p ATR-FTIR, Karlsruhe, Germany). A scanning electron microscope (SEM) (KYKY EM 3200, KYKY Co, Beijing, China) was used to obtain SEM images for the characterization of the diatom morphology including shape, structure, and size.

Cell culture

The HepG2 cell line (Life Technologies, Zug, Switzerland) was maintained at 37°C 5% $CO_2$. The Dulbecco's modified Eagle medium (Life Technologies, Zug, Switzerland) containing 1000 g/mL glucose was further supplemented with 10% fetal bovine serum (FBS) (Life Technologies, Zug, Switzerland), 100 U/mL of penicillin (Sigma-Aldrich, Buchs Switzerland), and 100 μg/mL of streptomycin (Sigma-Aldrich, Buchs, Switzerland). The Jurkat cell line (Life Technologies, Zug, Switzerland) was cultured in RPMI 1600 medium at 37°C ($CO_2$ 5%). All cell suspensions were filtered with a 45μm Cell Strainer Snap Cap (Fisher Scientific, Reinach, Switzerland) before each experiment.

**Cell conjugation to magnetic diatom frustules functionalized with the TLS11a aptamer**

$5\times10^5$ cells were cultured and incubated with 100μl of TLS11a-mag@DF (0.1 g/l) in a binding buffer (4.g/L glucose and 5mM $MgCl_2$) for 1h at room temperature. Then the suspension was washed three times with PBS before each experiment. According to the findings of previous studies, the aptamer TLS11a is able to bind to the surface of cancer cells with a high affinity [5].

**Numerical settings for the computational simulations**

In order to maximize the impact of the magnetic separation, computational simulations were performed to determine the correct location and intensity of the magnetic field within the microfluidic channel. The ideal 2D model for the magnetic separation part was created using the computer-aided-design modeler Rhinoceros 3D (v.7, Robert McNeel & Associates, Seattle, WA, USA). The computational domain consisted only the second separation part of the microfluidic device, where the magnetic separation of CTCs is expected to occur. Initially the geometrical model of the magnetic separation part was discretized into tetrahedral elements (with a minimum size of 0.001mm), with a prismatic layer made of 15 layers (exponential growth rate of 1.2). Following a mesh-independence analysis, the final mesh resulted in 129085 nodes and 127449 elements (Table S1). Both fluid dynamics and magnetic field steady-state simulations were performed in Ansys Fluent (v.2020, Academic, Ansys Inc., Canonsburg, PA, USA). The magneto-hydrodynamic (MHD) module was integrated with the solution of the Navier-Stokes equations to investigate the magneto-fluid dynamics of the cells

conjugated to magnetic nanoparticles. The convergence for the continuity and momentum, residuals value was set to $1\times10^{-5}$, with a maximum number of 1000 iterations, as defined from the residual sensitivity analysis. The final numerical settings were selected by performing various simulations and analyzing the values of wall shear stresses and min and max velocities for each one. The Pseudo-transient CFD simulations were performed within a coupled scheme namely compute pressure and velocity simultaneously. The numerical settings are reported in Table S1. Regarding the fluid boundary conditions, a flat inlet velocity derived from the experimental conditions was set to 0.004 m/s. A traction-free condition was imposed at the outlet sections, while the no-slip condition was assumed for the walls. The fluid material, presented as a mixture of human blood and PEO 0.1%, was modeled as a Newtonian fluid with a combined zero viscosity of 0.005 Pa s and a density of 1028 kg/m$^3$.

After computing the fluid field distribution, the magnetic field was calculated from the solutions of the MHD equations in conjunction with the influence of the Lorentz force on the cells. According to the specifications of the employed magnets in the experimental setup, we defined a value of 10T for the y-component of the external field B0. In this model, the fluid permeability was set as $1.27\times10^{-7}$ in accordance with a previous study.[5] By testing the influence of the boundary conditions on the strength of the magnetic field, the locations along the bottom wall of the schematic model (Figure S5A) were defined as conducting walls, in agreement with the experimental setup. All the other wall segments were defined as insulated. Finally, in order to track the CTCs, a discrete phase composed of inert, spherical particles of 20μm diameter was introduced.

## 2. Supporting Tables

**Table S1: Description of numerical settings used in the magneto-hydrodynamic (MHD) module**

| | |
|---|---|
| Type | Ansys CFX-pressure-based |
| Pleasure velocity coupling method | coupled |
| Special discretization scheme-gradient | Least squares cell based |
| Special discretization scheme-pressure | Second order |
| Special discretization scheme-momentum | Second order upwind |
| Special discretization scheme $B_X$ and $B_y$ | Second order upwind |
| Convergence criterion for the global residuals | $10^{-5}$ |

## 3. Supplementary text

### Characterization of magnetic nanoparticles and frustule morphology

SEM images of magnetic nanoparticles are depicted in Figure S1. As can be observed, the synthesized magnetic nanoparticles have a uniform spherical morphology with a size of 17 nm. Frustule morphology was characterized using scanning electron microscopy (SEM) (Figure S2). The Chaetoceros sp. frustules were divided into two parts: the hypotheca (Figure S2B), a Petri dish-like structure that is primarily responsible for their optical properties, and

the setae (Figure S2 C and D), which are thin, long and spin-like structures with several selves arranged nanopores linked to the hypotheca. The size of Setae frustules was approximately 2-4 μm, having pore sizes of 10×35 nm.

**Flow cytometric analysis of TLS11a specificity**

Flow cytometry was used to demonstrate the specificity of the TLS11a aptamer conjugated to diatom frustules (TLS11a-mag@ DF) against the HepG2 cells. Jurkat cells were employed as a negative control cell sample. This aptamer is known to target HepG2. Both Jurkat and HepG2 cells were incubated under the same TLS11a-mag@DF concentration. After incubation of TLS11a-mag@DF with Jurkat cells, no noticeable shift in the fluorescence signal is observed. However, incubation of HepG2 cells with TLS11a-mag@DF gives a considerable fluorescence shift, confirming the specificity of the TLS11a aptamer probe (Figure S7).

Computational analysis of the chip.

As shown in Figure S5 the presence of the magnetic field ($\Gamma_{con}$: conducting wall) in the vicinity of the bifurcation induces a deviation in the flow of the magnetic functionalized cells. In the absence of the magnetic field, the cells enter the top channel, which has a lower hydrodynamic resistance. However, after enabling the MHD module, cells enter the bottom channel as observed in the experiments. Simulations in Figure S5B, predict that the velocity field in the presence of a magnetic field remains the same along the whole microfluidic channel confirming that the presence of the magnets do not affect the flow. Finally the intensity of the magnetic field (Figure S5C) is sufficient to create an effective cell separation by driving the magnetic cells into the bottom channel.

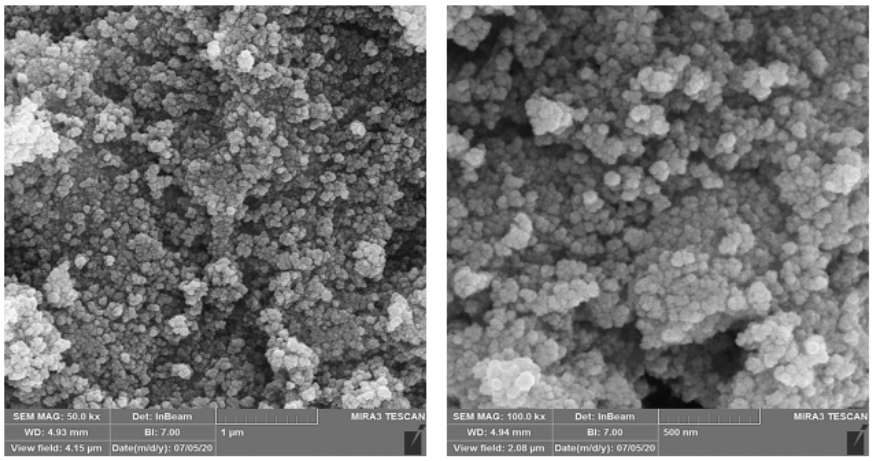


**Figure S1**. SEM images of magnetic nanoparticles. The magnetic nanoparticles have a uniform spherical morphology with sizes between 17 and 20nm. Scale bars are 1µm and 500nm on the left and right image respectively.

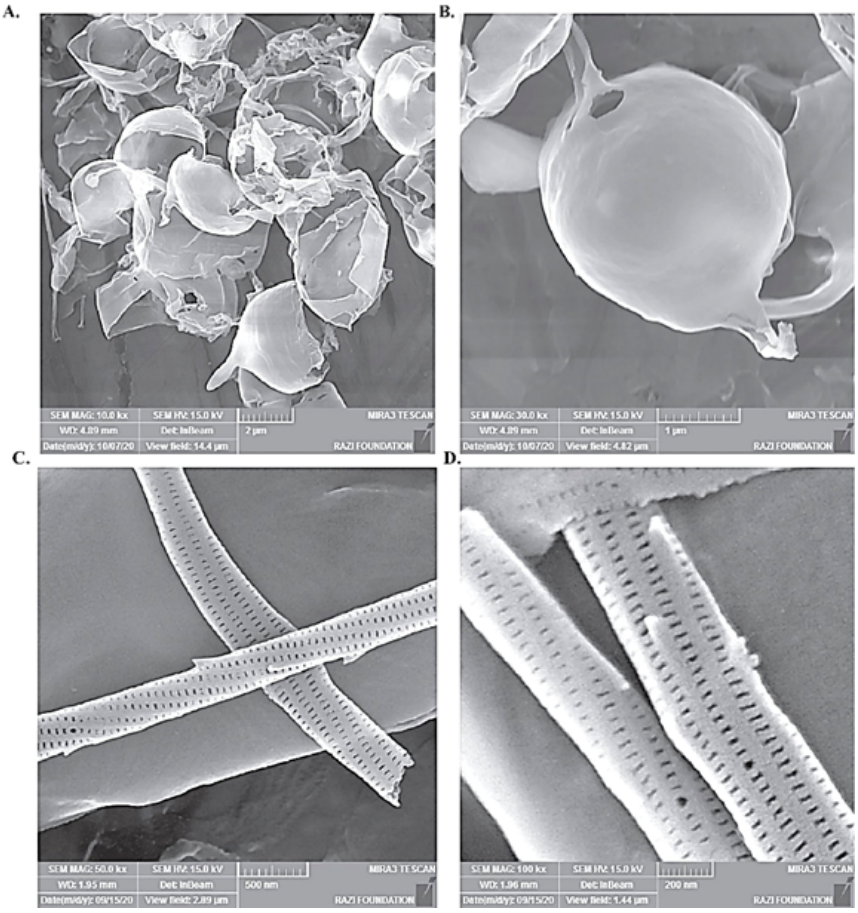


**Figure S2**. SEM images of diatom frustules morphology. (A) The overview of the frustule structure in a 2-µm scale bar. (B) The Hypotheca structure of diatom frustules. (C) The Setae structure of diatom frustules and a zoomed image of the structure (D) with a pore size of ~10 × 35nm.

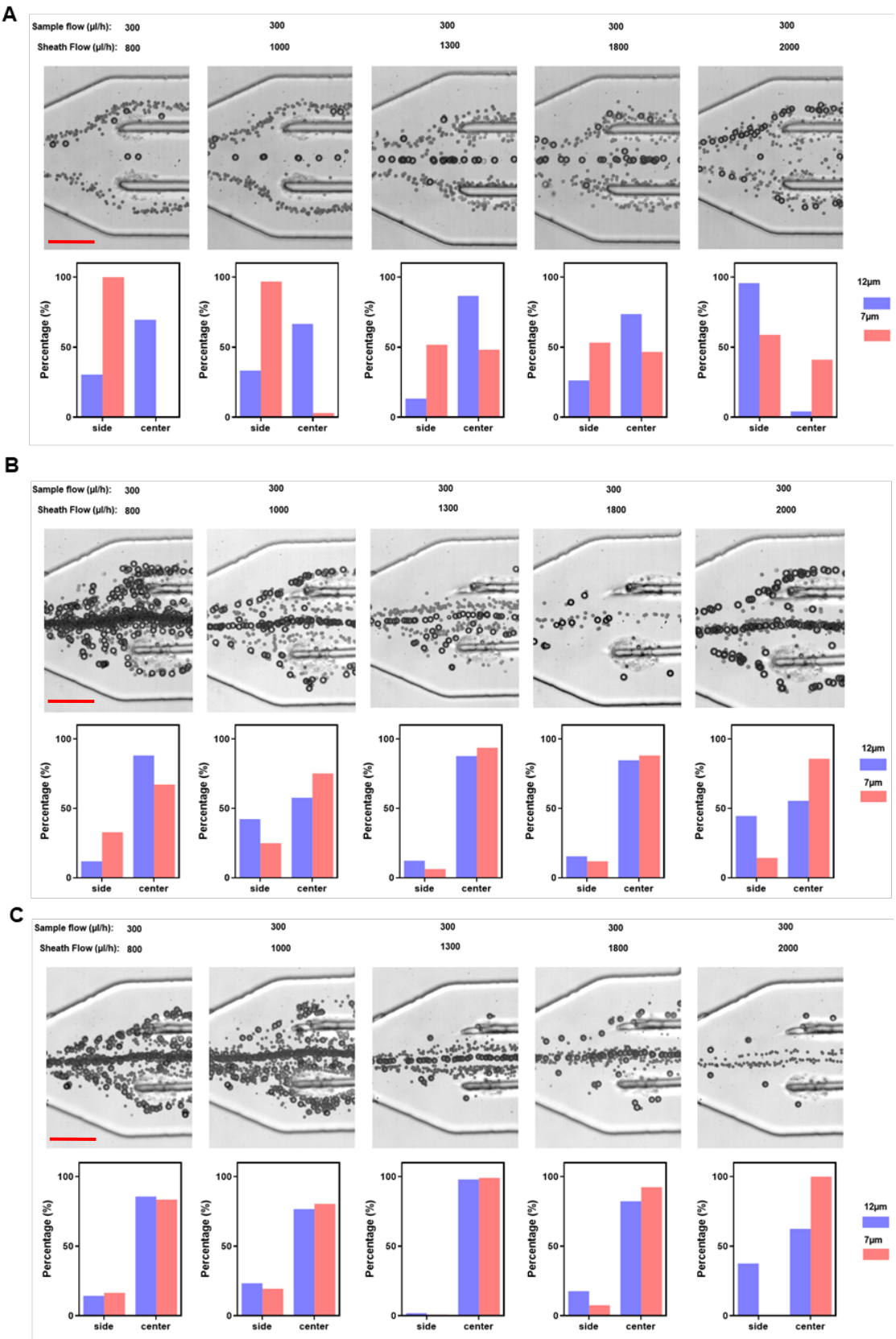


**Figure S3**. Brightfield images of the first part of the hybrid microfluidic device (top panel) and bar charts showing the separation efficiency for 7 and 12 µm polystyrene beads at different sample: sheath flow rate ratios and different PEO concentrations. (A) 0.15% PEO in sample flow and 0.3% PEO in sheath flow. (B) 0.2% PEO in sample flow and 0.3% PEO in sheath flow; (C) 0.25% PEO in sample flow and 0.3% PEO in sheath flow. Scale bars: 50mm.

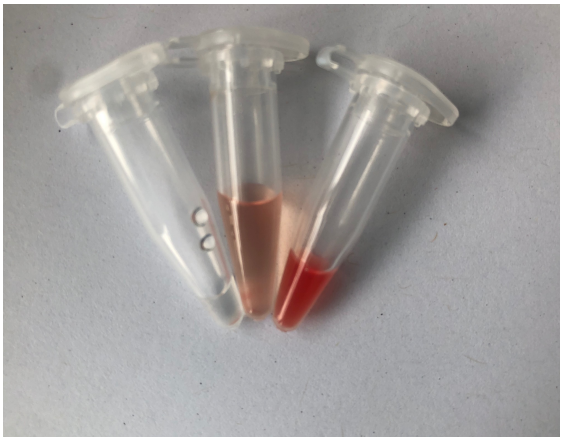

**Figure S4**. The content of each collected sample from the center outlet: CTCs+WBCs, (left tube), side outlet: RBCs, (middle tube). The inlet consists of whole blood +sheath fluid (right tube).

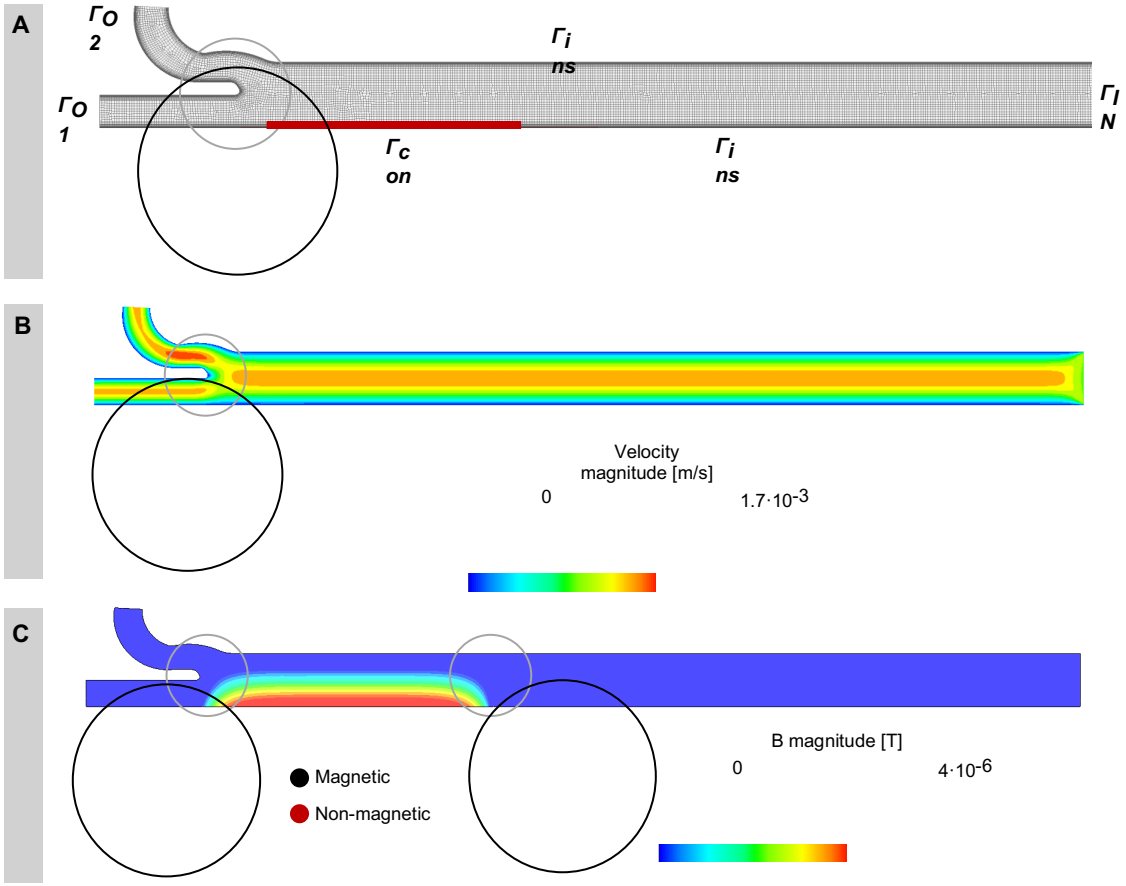


**Figure S5**. Computational model of the chip. A) Computational domain discretized in prismatic elements showing in detail the bifurcation region. $\Gamma_{con}$ : conducting wall; $\Gamma_{ins}$ : insulating wall; $\Gamma_{IN}$ : inlet; $\Gamma_{O1}$ : outlet 1; $\Gamma_{O2}$ : outlet 2. B) Velocity field distribution obtained from the computational fluid dynamics (CFD) pseudo-transient simulation, showing in detail the bifurcation region. C) The magnetic field B having an initial value of 10 T. Two particle flow paths are shown; in the case of magnetic particles (black) which are activated by the presence of the magnets and non-magnetic particles which are unaffected by the magnetic field (red).

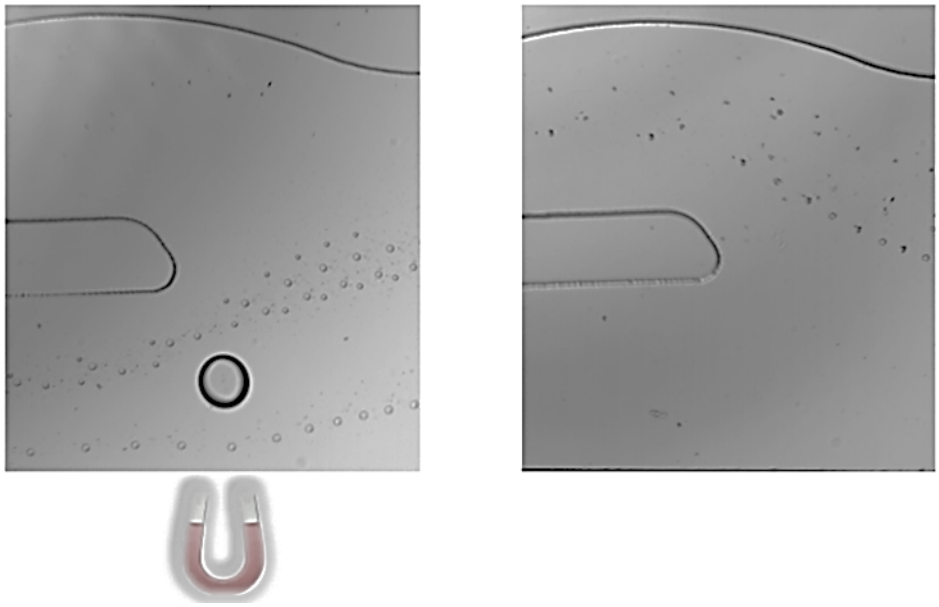

**Figure S6**. Magnetic migration of the HepG2 cells functionalized with magnetic diatom frustules spiked in 0.1% PEO. In the presence of a neodymium magnet cells are pulled toward the magnet (left image) whilst in the absence of the magnet, cells are flowing to the less hydraulic resistance channel (right image). The sheath flow in both experiments was 0.3% PEO.

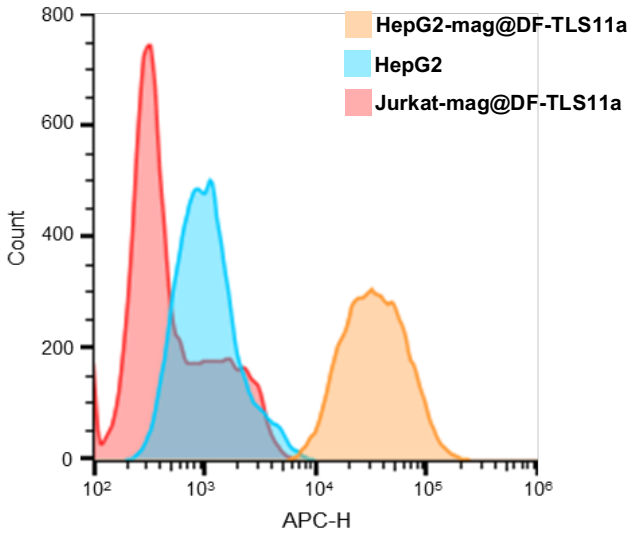


**Figure S7**. Detection of HepG2 CTCs before (cyan) and after conjugation with mag@DF-TLS11a (orange). Jurkat CTCs were used as control sample. No shift in the fluorescent intensity was observed when Jurkat cells were incubated with mag@DF-TLS11a (pink).

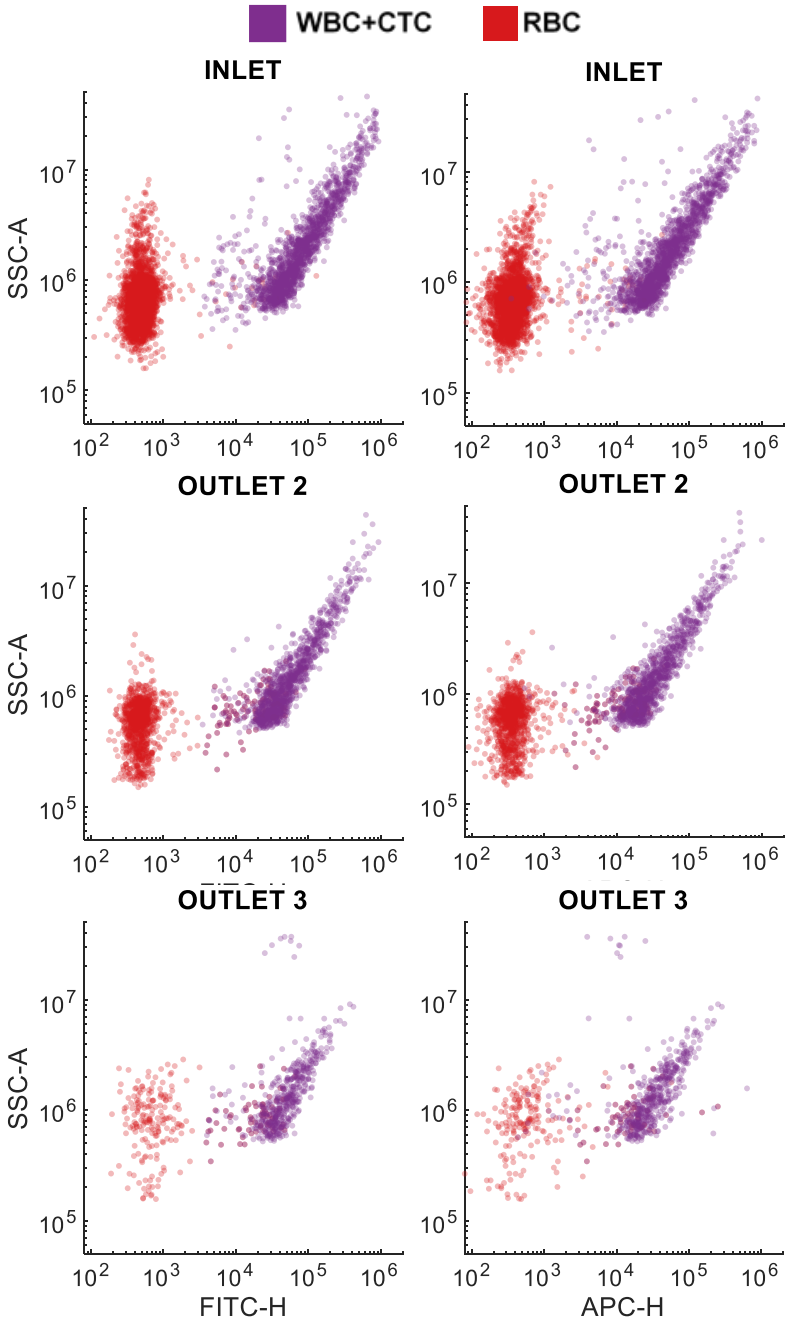


**Figure S8**. Particle separation results using flow cytometry scatter plots. Flow cytometry analysis of RBCs, and WBCs+CTCs populations at the inlet and outlets 2 and 3. Flow cytometry SSC vs FITC or APC graphs showing the ratio of RBCs (red), and WBCs+CTCs (blue) in the total mixture. In this graphical representation using only one fluorescent channel (either APC or FITC) CTCs cannot be discriminated from WBCs.

**References:**


(1) Radfar, I.; Kazemi Miraki, M.; Esfandiary, N.; Ghandi, L.; Heydari, A. Fe3O4@SiO2-Copper Sucrose Xanthate as a Green Nanocatalyst for N-, O- and S-Arylation. *Applied Organometallic Chemistry* **2019**, *33* (1), e4619. https://doi.org/https://doi.org/10.1002/aoc.4619.

(2) Esfandyari, J.; Shojaedin-Givi, B.; Hashemzadeh, H.; Mozafari-Nia, M.; Vaezi, Z.; Naderi-Manesh, H. Capture and Detection of Rare Cancer Cells in Blood by Intrinsic Fluorescence of a Novel Functionalized Diatom. *Photodiagnosis and Photodynamic Therapy* **2020**, *30*, 101753. https://doi.org/10.1016/j.pdpdt.2020.101753.

(3) Bayramoglu, G.; Akbulut, A.; Yakup Arica, M. Immobilization of Tyrosinase on Modified Diatom Biosilica: Enzymatic Removal of Phenolic Compounds from Aqueous Solution. *Journal of Hazardous Materials* **2013**, *244–245*, 528–536. https://doi.org/10.1016/j.jhazmat.2012.10.041.

(4) Yaroslav A. Grechkin1, Svetlana L. Grechkina2, Emil A. Zaripov1, Svetlana V. Fedorenko2, A. R. M. M. V. B. Aptamer-Conjugated Tb(III)-Doped SilicaNanoparticles for Luminescent Detection OfLeukemia Cells. **2020**, No. Iii.

(5) Lai, Z.; Tan, J.; Wan, R.; Tan, J.; Zhang, Z.; Hu, Z.; Li, J.; Yang, W.; Wang, Y.; Jiang, Y.; He, J.; Yang, N.; Lu, X.; Zhao, Y. An “activatable” Aptamer-Based Fluorescence Probe for the Detection of HepG2 Cells. *Oncology reports* **2017**, *37* (5), 2688–2694. https://doi.org/10.3892/or.2017.5527.

(6) Mohamadi, R. M.; Besant, J. D.; Mepham, A.; Green, B.; Mahmoudian, L.; Gibbs, T.; Ivanov, I.; Malvea, A.; Stojcic, J.; Allan, A. L.; Lowes, L. E.; Sargent, E. H.; Nam, R. K.; Kelley, S. O. Nanoparticle-Mediated Binning and Profiling of Heterogeneous Circulating Tumor Cell Subpopulations. *Angewandte Chemie - International Edition* **2015**, *54* (1), 139–143. https://doi.org/10.1002/anie.201409376.